New nanowire heterostructures: SnO_2 nanowires epitaxial growth on Si bicrystalline nanowires

Junqing Hu,* Zhigang Chen, Rujia Zou and Yangang Sun

Received 27th May 2009, Accepted 12th August 2009
First published as an Advance Article on the web 2nd September 2009
DOI: 10.1039/b910489p

Combining thermal decomposition and evaporation of a mixed powder of SiO and SnO_2 under careful temperature control resulted in SnO_2 nanowires epitaxial growth on Si bicrystalline nanowires, forming new three layered radial Si–Si–SnO_2 nanowire heterostructures, which the nature of interfacial regions and phase boundaries are different from the characteristics of axial composite nanowires. Each Si–Si–SnO_2 composite nanowire has a uniform diameter along its whole length; the typical diameter of the nanowires ranges from 50 to 150 nm, and the diameters of Si bicrystalline nanowires and SnO_2 nanowires within a nanowire heterostructure are ~30–100 nm. These Si–Si–SnO_2 nanowire heterostructures display unique intensive green luminescence emission compared to that of UV emissions of the near-band edge of SnO_2.

Introduction

One-dimensional nanowire heterostructures (NHs) by assembling two semiconducting nanowires or nanotubes are of particular interest with respect to potential applications in nanoelectronics and nanophotonics.[1–4] However, compared with a considerable development in nanowire and nanotube preparation in homogeneous systems, there have been fairly limited reports on the rational design and successful fabrication of heterostructures within a given 1D nanostructure. Normally, the NHs generally fall into two types: axial (longitudinal) and radial NHs.[2] Axial semiconductor nanowire multi-heterostructures, *i.e.* nanowire superlattices, with composition modulations have been prepared based on controlled chemical vapor deposition (CVD) processes in the GaAs/GaP,[5] InAs/InP,[6] and Si/SiGe[7] systems. Other demonstrations of axial NHs containing ternary III–V materials, such as GaAsP,[8] InAsP,[9] or InGaAs,[10] further increase the potential for heterostructure applications. Regarding radial NHs, TiO_2/SnO_2 composite nanoribbons have been obtained through an epitaxial growth of TiO_2 nanoribbon on a SnO_2 nanoribbon (as a substrate) *via* a pulsed laser deposition.[11] In our study, we tried to use Si nanowires as one-dimensional nanoscale substrates for the growth of ZnS or ZnSe nanowires. The resulting products were side-to-side Si–ZnS, Si–ZnSe biaxial NHs, and ZnS–Si–ZnS triaxial NHs by a chemical vapor deposition method.[12] These NHs achieve an excellent epitaxial coherent interface between two sides or three layers of sub-nanowires, which show enhanced luminescence properties. Following our study, ZnO/Ge and ZnS/ZnO epitaxial biaxial NHs have also been grown by a CVD similar method.[13,14]

SnO_2, an n-type wide bandgap semiconductor, is a key functional material that has been extensively used for optoelectronic devices, gas sensors, transparent conducting electrodes, and catalyst supports.[15,16] In the present study, combining thermal decomposition and evaporation of a mixed powder of SiO and SnO_2 under careful temperature control, the Si bicrystalline nanowires formed in the first stage and were then used as a template for epitaxial growth of SnO_2 nanowires in the second stage, forming a new three layered radial Si–Si–SnO_2 NH, the nature of interfacial regions and phase boundaries of which are different from the characteristics of axial composite nanowires. Also, these layered Si–Si–SnO_2 NHs display unique intensive green luminescence emission compared to that of UV emissions of the near-band edge of SnO_2.

Experimental

The Si–Si–SnO_2 three layered radial NHs were grown using a high-temperature vacuum alumina tube furnace. A graphite crucible containing a mixed powder of SnO_2 (1.5 g) and SiO (1.0 g) was placed at the central region of the tube. Several strip-like alumina wafers ultrasonically cleaned in acetone were used as substrates and placed on a wide and long alumina plate, which was inserted downstream into the tube. The tube was sealed and then pumped down to a base pressure of 2×10^{-2} torr. A constant flow of Ar mixed with 10% H_2 was introduced into the tube at a flow rate of 100 sccm and a total pressure of ~400 torr during the fabrication process. The furnace was heated at a rate of 30 °C min^{-1} to 1250 °C and maintained at this temperature for 1.5 h, followed by further heating to and holding at 1400 °C for 1.5 h before it was finally cooled to room temperature. The collected products were characterized using X-ray powder diffraction (XRD; RINT 2200) with CuKα radiation and transmission electron microscopy (TEM; JEM-2100F), equipped with an X-ray energy dispersive spectrometer (EDS). Cathodoluminescence (CL) spectroscopy was carried out in high spatial resolution, low energy CL system and a thermal-field-emission scanning electron microscopy (TFE-SEM, Hitachi S4200).

State Key Laboratory for Modification of Chemical Fibers and Polymer Materials, College of Materials Science and Engineering, Donghua University, Shanghai, 201620, China. E-mail: hu.junqing@dhu.edu.cn

Results and discussion

An XRD pattern, Fig. 1, shows that the as-grown product is a composite material containing the tetragonal rutile structure of SnO_2 (JCPDS file: 41–1445; $a = 4.738$ Å and $c = 3.187$ Å) and diamond-cubic Si (JCPDS file: 27–1402; $a = 5.420$ Å). No characteristic peaks from other crystalline forms are detected in the XRD pattern. Detailed microstructures of the composite material will be further investigated using TEM, EDS, and electron diffraction (ED).

TEM image examination demonstrated the structures of the as-synthesized products. It is found that the products were SnO_2 monolithic nanowires, Si–SnO_2 composite nanostructures, and Si bicrystalline (singly-twined) nanowires, and with a relative abundance of 30, 50, and 20%, respectively. The SnO_2 nanowires and nanoribbons had the same characteristics as those reported before.[17,18] Herein, we focus on the characterization of Si–SnO_2 composite nanostructures. In a low-magnification TEM image in Fig. 2, the clear variation in contrast along the length suggests that the grown product appears to display sandwich like triaxial nanowire structures, which consist of one light-contrast layer and two dark-contrast layers, forming nanowire heterostructures. Each Si–SnO_2 composite nanowire has a uniform diameter along its whole length; the typical diameter of the nanowires ranges from 50 to 150 nm, and the diameters of Si bicrystalline nanowires and SnO_2 nanowires within a nanowire heterostructure are ~30–100 nm. Nano beam (with an electron nanoprobe of ~20 nm) EDS analysis indicates that the light-contrast layer is pure SnO_2 and the dark-contrast layers are composed of Si (shown below). In fact, in such an individual three-layered composite nanowire, the constituent Si nanowire is a bicrystalline structure, which has a clear grain boundary at the center along the length. Imaging variation in contrast along the length results from a slight bending of the wires, causing changes in transmitted intensity, as shown in Fig. 2a. Some of the Si bicrystalline nanowire' surfaces are not smooth, instead, many tiny steps or wave-like convexities exist along the length, Fig. 2b. The presence or absence of twins in the remaining wires cannot be established

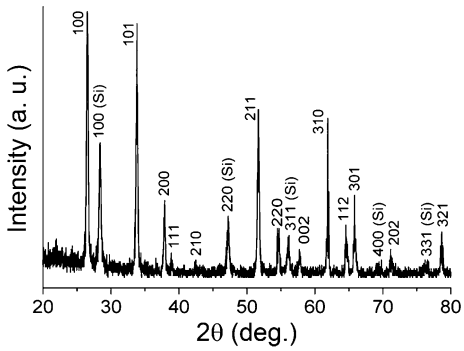

Fig. 1 XRD pattern recorded from the product.

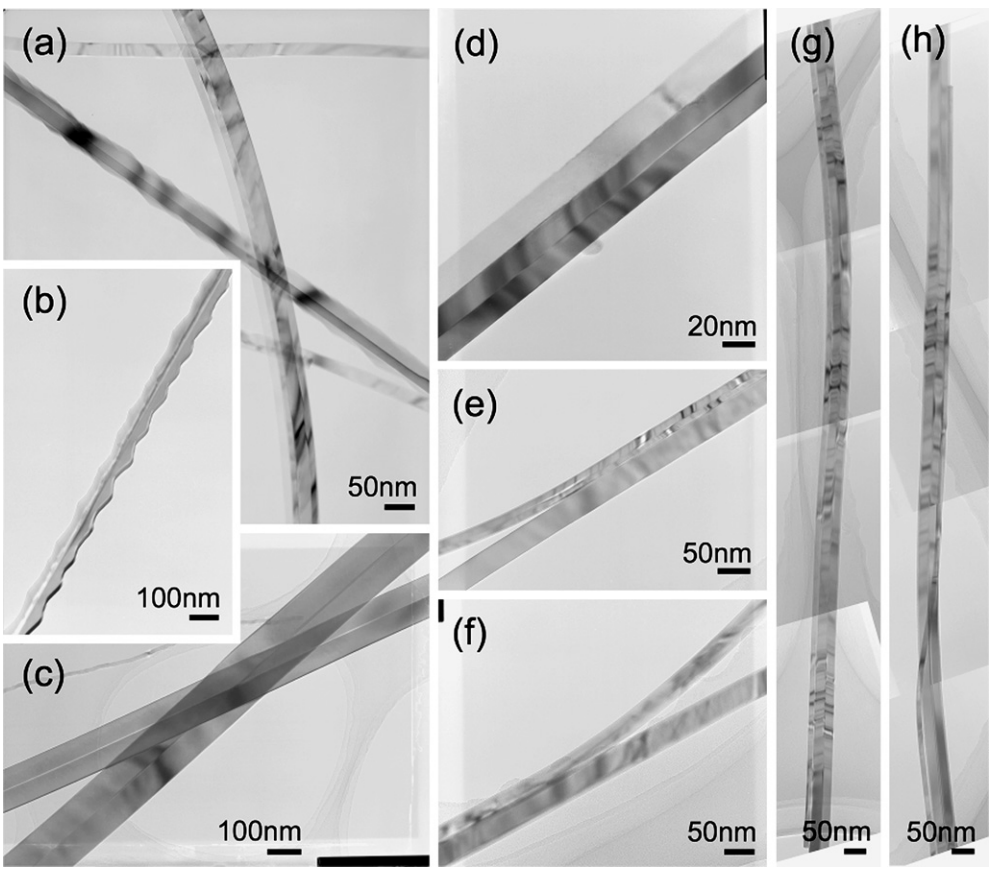

Fig. 2 Typical TEM images showing: (a) as-obtained radial layered Si–Si–SnO_2, (b), (c) wave-like and smooth Si bicrystalline nanowires, respectively, (d) a segment of a Si–SnO_2 NH, (e), (f) brunched Si–SnO_2 NHs, (g), (h) the entire lengths of the Si–SnO_2 NHs, the lengths can be longer than >10 μm.

definitively without tilting each wire to the appropriate zone axis orientation. As shown in Fig. 2c, the two Si smooth bicrystalline nanowires are aligned exactly with the electron beam perpendicular to the growth axis and parallel to the [1–10] zone axis. In this orientation, the (111) twins are viewed edge-on and can be seen along the entire length of the nanowires. A high-magnification TEM image in Fig. 2d clearly shows a SnO_2 nanowire growth on a Si bicrystalline nanowire, forming a new three layered Si–Si–SnO_2 NH whose nature of interfacial regions and phase boundaries is different from the characteristics of axial composite nanowires. In some cases, SnO_2 nanowires did not continuously grow on the Si bicrystalline nanowires, appearing to be a brunched NH, Fig. 2e and f. For a given Si–Si–SnO_2 NH, the geometry of a three layered structure is well maintained through the entire length (>10 μm), Fig. 2g, or terminated and brunched at the close end of this structure, Fig. 2 h.

Nano beam EDS spectra were collected from the Si bicrystalline nanowire part (Fig. 3a) and SnO_2 nanowire part (Fig. 3b), respectively. The spectrum in Fig. 3a reveals the presence of Si, Sn, and O (the Cu signal comes from a TEM grid). Quantization of the spectrum shows that the amount (wt%) of Si is as high as 70.6 (83.3 at%), and the contents of Sn and O are as low as 24.6 (6.8 at%) and 4.8 (9.9 at%), respectively, indicating the prime element Si of the Si sub-nanowire within the Si–Si–SnO_2 three layered NH. The spectrum in Fig. 3b is taken from the SnO_2 sub-nanowire, and indicates the presence of Sn (76.5 wt%; 31.9 at%) and O (19.8 wt%; 61.5 at%) (with an approximate stoichiometry of SnO_2) and a very low content of Si (3.7 wt%; 6.6 at%), suggesting the main compositions of Sn and O in the SnO_2 sub-nanowire within the Si–Si–SnO_2 three layered composite nanowire.

A high-magnification TEM, Fig. 4a depicts a segment of the Si–Si–SnO_2 three layered composite nanowire, which reveals a clear and uniform twined boundary and an interface between the Si and SnO_2 sub-nanowire layers. ED pattern, Fig. 4b, taken from the Si nanowire layer, is characteristic of a face-centered cubic material that is twined on {111}-type planes; in fact, it consists of overlapping patterns corresponding to the crystals on either side of the twin, and the individual patterns are determined as belonging to the [1–10] zone axis of a Si crystal. Streaking along the [111]* reciprocal lattice direction results primarily from

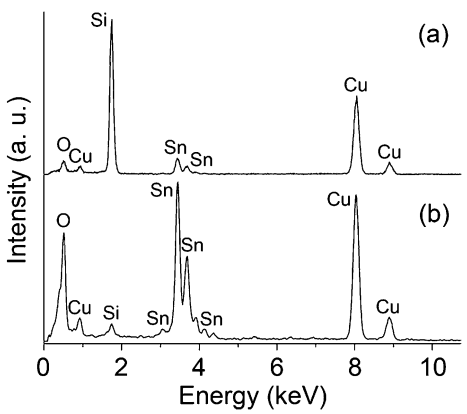

Fig. 3 Nano beam EDS spectra taken from Si bicrystalline sub-nanowire (a) and SnO_2 sub-nanowire (b), respectively, within a NH.

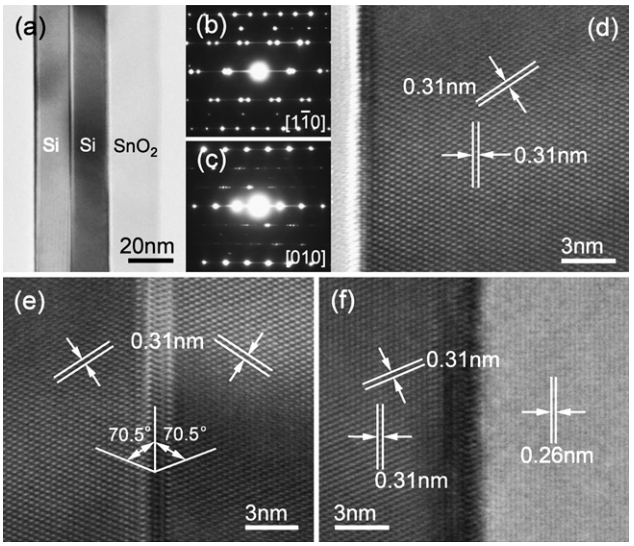

Fig. 4 (a) A high-magnification TEM showing a segment of the Si–Si–SnO_2 three layered radial NH. (b), (c) ED patterns taken from Si bicrystalline nanowire layer and SnO_2 nanowire layer, respectively. (d), (e) HRTEM image taken from the Si bicrystalline nanowire's surface and twined boundary, respectively. (f) HRTEM image of the Si–SnO_2 interface domain.

the limited number of scatters in this direction in the thin and fine nanowire. Fig. 4c, taken from the SnO_2 nanowire layer, can be indexed as the [010] zone axis diffraction pattern of the tetragonal rutile structure of the SnO_2 crystal. Fig. 4d is the HRTEM image taken from the Si nanowire layer surface. No dislocations or other planar defects are observed in it, and the marked interplanar d-spacings (of ~0.31 nm) correspond to that of the {111} lattice planes of the Si crystal. Significantly, (even though the sample was exposed to air for several months) the edge of the wire is clean and abrupt on an atomic scale, there are no amorphous sheathed phases attributed to oxidation observed on the surfaces commonly associated with Si nanowires.[19–22] A HRTEM image, Fig. 4e, taken from the Si bicrystalline nanowire within this NH, exhibits the twin characteristics of the Si nanowire. One set of the {111} planes is parallel to the interface plane on each side; another (indicated on the figure) shows a 141° angle (70.5° + 70.5°) between them and thus highlights the mirror symmetry. Further analysis indicates that this Si bicrystalline nanowire grows along the [11–2] direction, and the twining occurs along the [112] direction. ED pattern. An HRTEM image, Fig. 4f, is taken from the interface domain between the Si nanowire (left side) and SnO_2 nanowire (right side); it shows that the Si–SnO_2 interfaces are clean and uniform at the atomic scale and no amorphous layers are formed within them. The measured d-spacing of 0.26 nm is in agreement with those of the {101} crystallographic planes of SnO_2. After further analysis of the HRTEM image and ED pattern, an interfacial epitaxial relationship between the Si nanowire and SnO_2 nanowire is suggested, which is $(111)_{Si}//(101)_{SnO_2}$.

Fig. 5 shows a room temperature cathodoluminescence (CL) spectrum recorded from an individual Si–Si–SnO_2 three layered composite nanowire. One weak peak at 340 nm and two strong peaks at 395 and 494 nm are visible emissions from the SnO_2

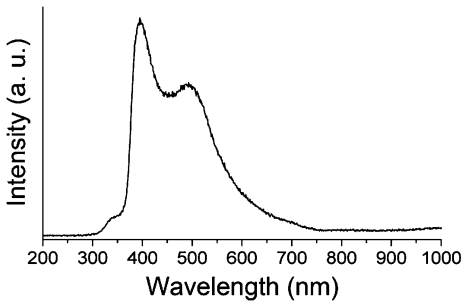

Fig. 5 Room-temperature CL spectrum of as-grown Si–Si–SnO_2 three layered radial NH.

nanowire layer, and no obvious emission peak is observed from the Si nanowire layer. The near-UV emission at 340 nm agrees with the band gap of bulk SnO_2 (Eg = 3.6 eV, at 300 K; 344 nm),[21,22] which comes from the recombination of free excitons.[23,24] The two strong emissions at 395 and 494 nm are comparable to the best values for SnO_2 thin films and SnO_2 nanowires.[18,25] They are related to the singly ionized oxygen vacancy, which may mainly locate on the surface of the nanowire, interact with interfacial tin vacancies, and lead to the formation of a considerable amount of trapped states within the bandgap.[23,24] These emissions result from the recombination of a photogenerated hole with a singly ionized charge state of the specific defect.[26]

The growth of the nanostructures discussed above was accomplished by combining a simple thermal decomposition and evaporation of a mixed powder of SiO and SnO_2 under careful temperature control. In the first stage, condensation of Si vapor due to thermal decomposition of SiO to Si + SiO_2 led to the growth of Si nanowires.[18,19] In the present case, a reduction atmosphere originated from 10% H_2 in the carrier gas and graphite crucible at the high processing temperature may be beneficial to the growth of Si bicrystalline nanowires; as-formed Si nanowires can resist significant oxidation and thus maintain fresh surfaces, otherwise the surface of the Si nanowires will be oxidized, forming Si/SiO_2 core-shell nanostructures.[18–21] The Si bicrystalline nanowires exhibit surface dangling bonds or surface dimer bonds or both, and the surfaces of the Si bicrystalline nanowires are energetically favorable. Thus, these Si bicrystalline nanowires can be used as one-dimensional substrates for conceivable vapor deposition processes. In the second stage, the adsorption or deposition of SnO_2 vapor due to thermal evaporating of SnO_2 will occur at the surfaces of these Si bicrystalline nanowire substrates. The nucleation of SnO_2 crystallites takes place epitaxially on the surfaces of Si nanowire substrates. The lattice rearrangement (from the diamond-cubic Si to tetragonal rutile SnO_2) easily occurs at the Si nanowire surface front, in particular, at the terraces having surface dangling bonds. The SnO_2 crystallites will grow on their lowest-energy faces {111}, parallel to those of the Si nanowires, forming the epitaxial relationship between the sub-nanowires of Si and SnO_2. In our experiment, it is found that the temperatures of 1250 °C at the first stage and 1400 °C at the second stage, respectively, are both optimized. If the durations of heating are both shorter than 1.5 h, this will reduce the yield of the products; if the durations of heating are both longer than 1.8 h, this has no significant effect on the yield and crystallinity of the products. The detailed growth mechanisms of the new nanostructures, however, are not fully understood, and require more systematic investigations.

Conclusion

In this contribution, by combining thermal decomposition and evaporation of a mixed powder of SiO and SnO_2 under careful temperature control, the Si bicrystalline nanowires formed in the first stage and were then used as a template for epitaxial growth of SnO_2 nanowires in the second stage, forming a new three layered radial Si–Si–SnO_2 NHs. Each Si–Si–SnO_2 NH has a uniform diameter along its whole length; the typical diameter of the nanowires ranges from 50 to 150 nm, and the diameters of Si bicrystalline nanowires and SnO_2 nanowires within a NH are ~30–100 nm. Also, these layered Si–Si–SnO_2 NHs display unique intensive green luminescence emission compared to that of UV emissions of the near-band edge of SnO_2, which may find applications in the photoelectric devices, fluorescence labels, and sensors. The present extended nanowire template method demonstrated here could be developed into a general approach of fabricating NHs made of Si-based materials.

Acknowledgements

This work was supported by the Program for New Century Excellent Talents of the University in China, the "Pujiang" Program of Shanghai Education Commission, China (Grant No. 09PJ1400500), the "Dawn" Program of Shanghai Education Commission, China (Grant No. 08SG32), the National Natural Science Foundation of China (Grant No. 50872020), the Program for the Specially Appointed Professor by Donghua University (Shanghai, P. R. China), Shanghai Leading Academic Discipline Project (Grant No. B603), and the Program of Introducing Talents of Discipline to Universities (Grant No. 111-2-04).

References

1 S. M. Sze, *Physics of Semiconductor Devices*, Wiley-Interscience, New York, 1981.
2 J. Q. Hu, Y. Bando and D. Golberg, *J. Mater. Chem.*, 2009, **19**, 330.
3 C. L. Jiang, F. Wang, N. Q. Wu and X. G. Liu, *Adv. Mater.*, 2008, **20**, 4826.
4 X. Liu, *Angew. Chem., Int. Ed.*, 2009, **48**, 3018.
5 M. S. Gudiksen, L. J. Lauhon, J. Wang, D. C. Smith and C. M. Lieber, *Nature*, 2002, **415**, 617.
6 (*a*) M. T. Björk, B. J. Ohlsson, T. Sass, A. I. Persson, C. Thelander, M. H. Magnusson, K. Deppert, L. R. Wallenberg and L. Samuelson, *Appl. Phys. Lett.*, 2002, **80**, 1058; (*b*) M. T. Björk, B. J. Ohlsson, T. Sass, A. I. Persson, C. Thelander, K. Magnusson, M. H. Deppert, L. R. Wallenberg and L. Samuelson, *Nano Lett.*, 2002, **2**, 87.
7 Y. Y. Wu, R. Fan and R. P. D. Yang, *Nano Lett.*, 2002, **2**, 83.
8 C. P. T. Svensson, W. Seifert, M. W. Larsson, L. R. Wallenberg, J. Stangl, G. Bauer and L. Samuelson, *Nanotechnology*, 2005, **16**, 936.
9 A. I. Persson, M. T. Björk, S. Jeppesen, J. B. Wagner, L. R. Wallenberg and L. Samuelson, *Nano Lett.*, 2006, **6**, 403.
10 I. Regolin, D. Sudfeld, S. Lüttjohann, V. Khorenko, W. Prost, J. Kästner, G. Dumpich, C. Meier, A. Lorke and F. J. Tegude, *J. Cryst. Growth*, 2007, **298**, 607.
11 R. He, M. Law, R. Fan, F. Kim and P. Yang, *Nano Lett.*, 2002, **2**, 1109.
12 J. Q. Hu, Y. Bando, Z. W. Liu, T. Sekiguchi, D. Golberg and J. H. Zhan, *J. Am. Chem. Soc.*, 2003, **125**, 11306.

13 L. W. Yin, M. S. Li, Y. Bando, D. Golberg, X. L. Yuan and T. Sekiguchi, *Adv. Funct. Mater.*, 2007, **17**, 270.
14 J. Yan, X. S. Fang, L. Zhang, Y. Bando, U. K. Gautam, B. Dierre, T. Sekiguchi and D. Golberg, *Nano Lett.*, 2008, **8**, 2794.
15 N. Yamazoe, *Sens. Actuators, B*, 1991, **5**, 7.
16 C. Nayral, E. Viala, V. Collière, P. Fau, F. Senocq, A. Maisonnat and B. Chaudret, *Appl. Surf. Sci.*, 2000, **164**, 219.
17 Z. W. Pan, Z. R. Dai and Z. L. Wang, *Science*, 2001, **291**, 1947.
18 J. Q. Hu, X. L. Ma, N. G. Shang, Z. Y. Xie, N. B. Wong, C. S. Lee and S. T. Lee, *J. Phys. Chem. B*, 2002, **106**, 3823.
19 N. Wang, Y. H. Tang, Y. F. Zhang, C. S. Lee and S. T. Lee, *Phys. Rev. B: Condens. Matter Mater. Phys.*, 1998, **58**, R16024.
20 W. S. Shi, H. Y. Peng, L. Xu, N. Wang, Y. H. Tang and S. T. Lee, *Adv. Mater.*, 2000, **12**, 1927.
21 A. M. Morales and C. M. Lieber, *Science*, 1998, **279**, 208.
22 J. L. Gole, J. D. Stout, W. L. Rauch and Z. L. Wang, *Appl. Phys. Lett.*, 2000, **76**, 2346.
23 A. Aoki and H. Sasakura, *Jpn. J. Appl. Phys., Part 1*, 1970, **9**, 852.
24 C. Tatsuyama and S. Ichimura, *Jpn. J. Appl. Phys., Part 1*, 1976, **15**, 843.
25 T. W. Kim, D. U. Lee and Y. S. Yoon, *J. Appl. Phys.*, 2000, **88**, 3759.
26 X. C. Wu, B. S. Zou, J. R. Xu, B. L. Yu, G. Q. Tang, G. L. Zhang and W. J. Chen, *Nanostruct. Mater.*, 1997, **8**, 179.